Ab initio molecular dynamics study of elasticity of akimotoite MgSiO$_3$ at mantle conditions

Li Li [a,b,∗], Donald J. Weidner [a,b], John Brodholt [a], Dario Alfè [a], G. David Price [a]

[a] Department of Earth Sciences, University College London, Gower Street, London WC1E6BT, UK
[b] Mineral Physics Institute, Department of Geosciences, University of New York at Stony Brook, Stony Brook, NY 11790, USA

ABSTRACT

The thermo-elastic properties of MgSiO$_3$ akimotoite at mantle pressure and temperature conditions are reported based on ab initio molecular dynamic simulations. A third-order Birch–Murnaghan equation at a reference temperature of 2000 K is defined by $K_0 = 158$ GPa, $K_0' = 3.7$, $G_0 = 85.7$ GPa, $G_0' = 4.5$, $V_0(2000\,K) = 1100.54$ Å^3, the Grűneisen parameter is determined to be $\gamma(V) = \gamma_0(V/V_0(2000\,K))^q$ with $\gamma_0 = 1.84$ and $q = 1.84$, with $V(2000\,K) = 1048.22$ Å^3. An implied pressure correction is -7.6 GPa in these parameters due to GGA overestimates the pressure. The thermal expansion is determined to be $\alpha/\alpha_0 = (V/V_0(2000\,K))^{\delta_T}$ in which $\alpha_0 = 3.21 \times 10^{-5}$ K^{-1} and $\delta_T = 4.6$. Akimotoite may be stable above the 660 discontinuity in relatively low temperature or low aluminium environments. The high velocity and elastic anisotropy of akimotoite provide diagnostics for its presence above the 660 km discontinuity.

Published by Elsevier B.V.

1. Introduction

The ilmenite form of MgSiO$_3$, akimotoite, is one of the possible phases in a pyrolitic mantle. It is stable at pressures (P) corresponding to the bottom of the transition zone, and at temperatures (T) of the cold subduction zone environment or low aluminium content (Gasparik, 1990; Ito and Yamada, 1982; Kawai et al., 1974; Tachimori et al., 1975), as shown in Fig. 1. The formation and annihilation of akimotoite occurs in the deep earth by the phase transformations from garnet and to perovskite (Ito and Yamada, 1982). The presence of akimotoite may not produce a seismic discontinuity (Weidner and Ito, 1985), although the akimotoite forming phase transition may introduce a high velocity region sitting on the 660 km discontinuity like a phantom slab (Weidner and Wang, 2000). With the major minerals above 660 discontinuity being nearly isotropic (Kiefer et al., 1997; Li et al., 2006a,c, 2007, submitted-a), the anisotropic characteristic of akimotoite is significant for interpreting seismic anisotropies in this region (Zhang et al., 2005). Thus, the knowledge of elastic properties of akimotoite is important for modelling the structure of the earth.

Our understanding of the structure of the mantle is constrained by seismic observations, in which the shear wave properties are crucial (Deuss and Woodhouse, 2001; Gossler and Kind, 1996;

Gu et al., 1998). Despite its importance, the shear properties of MgSiO$_3$ ilmenite at P–T conditions relevant to the earth have not been reported. The available experimental data are either limited to room P–T (Weidner and Ito, 1985) while high P–high T data are limited to Raman studies (Reynard and Rubie, 1996) or P–V–T measurements (Wang et al., 2004) with a lack of shear modulus constraints. A theoretical study using semi-empirical potentials predicted the structural and elastic properties of akimotoite (Matsui et al., 1987; Zhang et al., 2005). At 0 K, the elasticity of akimotoite was modelled using the ab initio pseudopotential method (Da Silva et al., 1999). The vibrational density of states (VDoS) of akimotoite was calculated at 0 K (Karki and Wentzcovitch, 2002) using the lattice dynamics approach, then the thermo-elasticity was derived using the quasiharmonic approximation.

In the recent few years, theoretical studies using the ab inito molecular dynamics (AIMD) approach, which simulates the stress–strain relation at elevated pressure and temperature conditions, has been shown to be an accurate method for calculating elastic properties at high pressure and temperature. It explicitly includes temperature in its simulation and has been used successfully to predict the structural and thermo-elastic properties of many mantle silicates (Li et al., 2006a, 2006b, 2006c, in press, submitted-a; Oganov et al., 2001a, 2001b). In this paper, therefore, we use the AIMD method to quantify the thermo-elasticity of akimotoite at mantle P–T conditions. We then explore the effect of the presence of akimotoite on the seismic velocity and anisotropy of the mantle.

∗ Corresponding author at: Mineral Physics Institute, Department of Geosciences, University of New York at Stony Brook, ESS bldg, Stony Brook, NY 11790, USA.
E-mail address: lilli@ic.sunysb.edu (L. Li).

2. Computation method

Akimotoite has a trigonal structure (R-3 space group), and is composed of MgO_6 and SiO_6 octahedral with shared faces. The atoms are in the following crystallographic sites: Mg(6c), Si(6c) and O(18f). Six-coordinated Mg and Si atoms form layers which alternate along the *c*-axis. The unit cell contains 6 formula units (30 atoms). All calculations were performed using a $2 \times 2 \times 1$ cell containing 120 atoms. The basis vector for this trigonal cell is $(2a \cos(\alpha), 0, 0)$, $(2a \sin(\alpha), 2a, 0)$ and $(0, 0, c)$, in which $\alpha = 60°$.

We used the VASP code to perform our AIMD simulations (Kresse and Furthmüller, 1996a, 1996b). We used the projector-augmented-wave (PAW) implementation of density functional theory (DFT) (Blöchl, 1994) and the implementation of an efficient extrapolation for the charge density (Alfè, 1999). We used the exchange–correlation functional E_{xc} in the PW91 form of the generalized gradient approximation (GGA) (Perdew et al., 1992; Wang and Perdew, 1991). The Γ-point was used for sampling the Brillouin zone. Using a cell with volume of 997 Å³ at 1500 K, our test showed that the pressure is 28.20 GPa using Γ-point calculation vs. 28.26 GPa using $2 \times 2 \times 2$ *K*-point calculation, thus the stress difference was negligible here even thought the $2 \times 2 \times 2$ *K*-point calculation required significantly longer computation power. Furthermore, elastic constants are insensitive at same conditions between gamma point and $2 \times 2 \times 2$ *K*-point calculation. The elastic constants were calculated at three volumes (1087.6 Å³, 1037.2 Å³ and 997.0 Å³). At each volume, three temperatures are considered (1500 K, 2000 K and 3000 K). The plane-wave cut-off energy 600 eV is adequate as the effect of using a larger cut-off is found to be insignificant. At elevated temperatures, lattice parameters were fixed and the ionic positions were allowed to relax. The core

radii were 2.0 a.u. for Mg (core configuration $1s^2 2s^2$), 1.5 a.u. for Si ($1s^2 2s^2 2p^6$) and 1.52 a.u. for O ($1s^2$). The equilibrium structure was obtained after at least 2ps of simulation. Error analysis for all pressures was done by reblocking the data, as described by previous studies (Allen and Tildesley, 1997). This reblocking method allows one to check when the calculations are efficiently long to reach required precision. Our stress error bar is within 0.5 GPa. Four configuration of strains (−1%, 1%) were applied to the equilibrated structure in order to derive 7 non-redundant c_{ij}; the resulted stresses were calculated over at least 1ps of simulation. The linearity of stress vs. strain was carefully checked when elastic moduli were derived.

## 3. Results and discussion

3.1. Elastic constants at 0 K

A 120-atom cell with R-3 symmetry atom positions was used in these calculations. We defined the relaxed atom positions and calculated the elastic constants at 0 K and room pressure which we can compare with the reported results (Matsui et al., 1987; Weidner and Ito, 1985) as listed in Table 1. Our results are consistent with the experimental results of the previous study (Weidner and Ito, 1985), as are the previously reported calculations (Da Silva et al., 1999; Matsui et al., 1987). The differences among the two calculations are to be expected owing to the different exchange–correlation potential used.

It is well known that even though GGA generally yields very accurate elastic moduli, it tends to overestimate the pressure when compared with experiments. Since GGA reproduces accurate elastic properties at each volume, we can obtain the correct pressure dependence of the volume by adjusting the GGA pressure to match the true $P(V)$ dependence following $P_{total}(V, T) = P_{GGA}(V) + P_{th}(V, T) - \Delta P$ (Oganov et al., 2001a). Using $V_0 = 1048.22$ Å³ (Weidner and Ito, 1985) and EOS fitting, we derived $K_0 = 223$ GPa and $K' = 4.2$ with an estimate of $\Delta P = 7.6$ GPa. Our previous studies have shown that this offset is insensitive to P and T (Li et al., in press). In the following text, we use the corrected pressure (P_c) to represent the pressure term, $P_c = P_{GGA} - 7.6$ GPa where P_{GGA} is the pressure calculated from GGA model.

3.2. Thermo-elasticity

We have calculated the single-crystal elastic constants, bulk moduli and shear moduli at three volumes, 1087.6 Å³, 1037.2 Å³ and 997.0 Å³, and three temperatures, 1500 K, 2000 K and 3000 K. These are listed in Table 2. We see that the bulk modulus is temperature independent, at constant volume, within the uncertainty of the calculation; the shear modulus, however, decreases with temperature at constant volume with $(\partial G/\partial T)_V = -0.010(5)$ GPa K⁻¹ indicating anharmonic contributions to the shear modulus.

The thermal parameters are calculated and listed in Table 3. Thermal expansion α is obtained from $(\partial P/\partial T)_V/K_T$. Since the bulk modulus K_T is insensitive to temperature at constant volume within the error of calculated pressure, the thermal expansion also becomes temperature insensitive at constant volume in the calculated P–T conditions. The Grüneisen parameter, $\gamma(V)$, is calculated from the thermal pressure and thermal energy: $\gamma(V) = P_{th}(V, T)V/E_{th}(V, T)$, where the thermal energy $E_{th} = 3(N-1)k_bT$, with k_b is the Boltzmann constant, N is the number of atoms in the supercell ($N = 120$ in this study). As we can see in Table 3, the dependence of $\gamma(V)$ on temperature is insignificant. Since our calculations are mostly at high temperature (above the Debye temperature) and the Earth's mantle is also at high temperature, we define the refer-
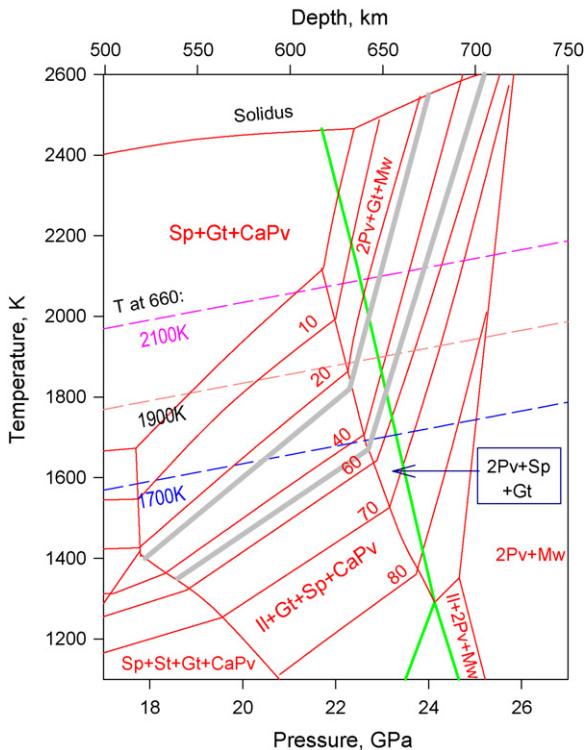
Fig. 1. Phase diagram of the CMAS system (CaO–MgO–Al₂O₃–SiO₂) modified after Gasparik (1990) with Gt, garnet; Sp, spinel; or ringwoodite; CaPv, CaSiO₃ perovskite; Pv, MgSiO₃ perovskite; Mw, magnesiowustite; St. stishovite; Il, MgSiO₃ in the ilmentite phase or akimotoite. Thick solid curves indicate the phase boundaries of the olivine normative system. The numbers on the thin solid curves indicate the pyrope content of the garnet in equilibrium with the other phases. Dashed curves indicate possible geotherms with labels that indicate the temperature at 660 km depth.

Table 1

Static condition (0 K) elastic moduli (c_{ij}), bulk moduli (K) and shear moduli (G) in GPa of MgSiO$_3$ ilmenite, compared with experimental data (T = 300K) a: (Weidner and Ito, 1985) and pervious calculations, b: (Da Silva et al., 1999), c: (Matsui et al., 1987) and d: (Zhang et al., 2005).

	P (GPa)	c_{11}	c_{12}	c_{13}	c_{14}	c_{33}	c_{44}	c_{25}	K	G
This study	−7.5	418	140	70	−24	337	92	−18	190	117
This study	2.4	479	170	109	−30	397	115	−14	234	134
This study	12.3	530	201	144	−35	444	134	−13	274	147
Ref a experiment	0.0	472	168	70	−27	382	106	−24	212	132
Ref b calculation	0.0	477	153	89	−28	392	121	−16	222	144
Ref c calculation	0.0	444	173	122	−24	383	90	−28	234	120
Ref d calculation	0.0	476	155	102	−29	383	114	−26	226	136

Table 2

Single-crystal elastic constants c_{ij} (GPa), bulk modulus (K, GPa), shear modulus (G, GPa) at elevated P and T. The volume (V) represents four unit cells (120 atoms). RVH represent the Reuss–Voigt–Hill average.

	V = 1087.6 Å^3			V = 1037.2 Å^3			V = 997.0 Å^3		
T (K)	1500	2000	3000	1500	2000	3000	1500	2000	3000
P_c (GPa)	0.9(2)	4.1(3)	12.5(4)	10.8(2)	13.8(2)	19.7(4)	20.6(2)	23.7(5)	29.5(5)
c_{11}	380	359	391	456	443	413	513	516	486
c_{12}	159	145	156	178	176	187	204	209	246
c_{13}	89	73	104	130	123	102	157	162	141
c_{14}	−27	−29	−31	−23	−27	−24	−40	−40	−30
c_{33}	319	351	290	378	372	515	439	422	411
c_{44}	79	59	59	101	98	89	123	120	103
c_{25}	−18	−18	−18	−16	−18	−18	−16	−14	−19
K_{Reuss}	190	182	192	237	230	236	275	275	264
K_{Voigt}	86	66	65	115	108	100	124	121	105
G_{Reuss}	195	183	200	241	234	236	278	280	271
G_{Voigt}	103	97	94	125	122	122	143	140	122
K_{RVH}	192	182	196	239	232	236	276	277	267
G_{RVH}	94	82	80	120	115	111	134	131	114

Table 3

Thermal expansion (α), Grüneisen parameter (γ), thermal pressure (P_{th}) at high pressure and temperature (T). P_c is the corrected pressure; $P_c = P_{GGA} - 7.6$ GPa. The volume (V) represents four unit cells (120 atoms).

V (Å^3)	T (K)	P_c (GPa)	P_{th} (GPa)	$(\partial P/\partial T)_V$ (GPa K^{-1})	α ($\times 10^{-5}$ K^{-1})	Γ
1087.6	1500	0.9	8.5	0.0058	3.05	1.25
1087.6	2000	4.1	11.7			1.30
1087.6	3000	12.5	20.1			1.48
1037.2	1500	10.8	8.5	0.0057	2.42	1.19
1037.2	2000	13.8	11.5			1.21
1037.2	3000	19.7	17.4			1.22
997.0	1500	20.6	8.3	0.0056	2.05	1.12
997.0	2000	23.7	11.4			1.15
997.0	3000	29.5	17.2			1.16

ence condition for all of the equation of state parameters as zero pressure and 2000 K. Using $V_0(2000\,K) = 1100.5\,Å^3$ to fit the relation: $\gamma = \gamma_0(2000)(V/V_0(2000))^q$, we obtain $\gamma_0 = 1.36$ and $q = 1.84 \pm 0.05$. The Anderson Grüneisen parameter, δ_T, is given by $\delta_T = (\partial \ln \alpha / \partial \ln V)_T$. Our best fit values are $\delta_T = 4.59 \pm 0.05$ and $\alpha_0 = 3.21 \times 10^{-5}$, K^{-1} referred at 2000 K.

Finally, we fitted the P–T data and the K_T–T data calculated for the three volumes at three temperatures with a third-order Birch–Murnaghan equation of state, using $(\partial K/\partial T)_V = 0$ and $V(2000\,K)$ as the reference volume. We fit the Reuss–Voigt–Hill averaged shear modulus with a third-order Eulerian strain equation of state. The best fit is for $G(2000\,K)$ of 85.7 GPa and $\partial G/\partial P$ of 4.5. The derived the equation of state parameters given in Table 4. Using parameters in Table 4, we fit the third-order Birch–Murnaghan equation of state to derive the isothermal P–V relation at 0 K, 300 K, 1000 K, 1500 K and 2000 K, as shown in Fig. 2. Also plotted are the experimental data measured at room temperature (Reynard et al., 1996) and at high P–high T (Wang et al., 2004). Our calculated 300 K EOS agrees with the room temperature data from both studies excellently. The data measured at high temperature (Wang et al., 2004) are also well described by our equation of state. They have a single point above 1000 K which is measured at 17 GPa and 1373 K; the rest of the data measured at temper-

ature from 298 K to 773 K are in-between our 300–1000 K P–V relation.

3.3. Anisotropy

The compressibility of akimotoite along the c-axis differs from that of the a-axis as observed in the experiments (Reynard et al.,

Table 4

Equation of state parameters with reference condition at 0 GPa and 2000 K. A third-order Birch–Murnaghan fitting of the AIMD bulk modulus vs. volume and corrected-pressure vs. volume yield these 2000 K reference state variables.

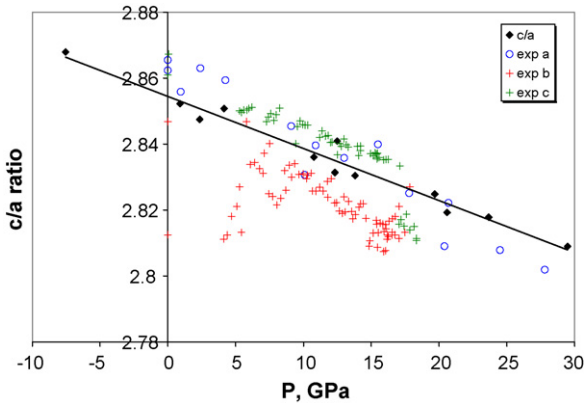| Property	Akimotoite
$V(2000\,K)$ (Å^3)	1100.5(4)
$\alpha \times 10^{-5}$ (K^{-1})	3.21(3)
δ	4.59(3)
γ	1.36(3)
q	1.84(3)
K_T^0 (GPa)	158.1(6)
$(\partial K_T/\partial P)_T$	3.7(2)
$(\partial K_T/\partial T)_V$ (GPa K^{-1})	0
G^0 (GPa)	85.7
$(\partial G/\partial P)_T$	4.5(3)
$(\partial G/\partial T)_V$ (GPa K^{-1})	−0.010(5)

Table 5
Maximum and minimum acoustic velocities.

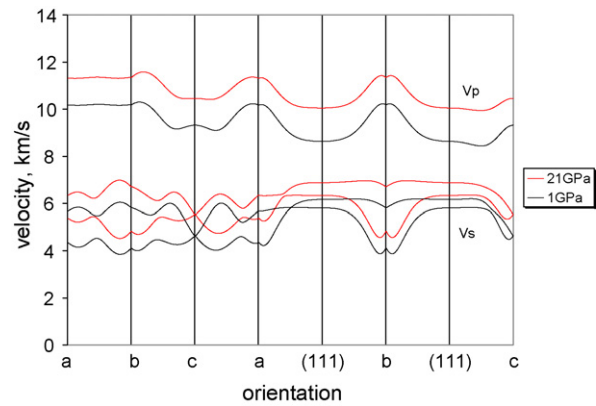| V (Å^3)	T (K)	MAXV$_P$	MINV$_P$	MAXV$_S$	MINV$_S$	MAXV$_P$/MINV$_P$	MAXV$_S$/MINV$_S$	SSPLIT
	0	10.66	9.17	6.43	5.01	1.16	1.28	1.23
	1500	10.16	8.93	5.93	4.63	1.14	1.28	1.18
1087.6	2000	10.87	9.74	6.07	5.13	1.12	1.18	1.17
	3000	11.31	10.36	6.28	5.54	1.09	1.13	1.12
	0	11.14	9.92	6.50	5.46	1.12	1.19	1.16
	1500	9.88	8.61	6.19	4.00	1.15	1.55	1.35
1037.2	2000	10.71	9.61	6.04	5.04	1.11	1.20	1.17
	3000	11.34	10.22	6.19	5.47	1.11	1.13	1.13
	0	11.50	10.44	6.51	5.77	1.10	1.13	1.11
	1500	10.31	8.57	5.65	4.00	1.20	1.41	1.41
997.0	2000	11.55	9.73	6.80	4.80	1.19	1.42	1.33
	3000	11.01	9.87	6.17	5.07	1.12	1.22	1.18
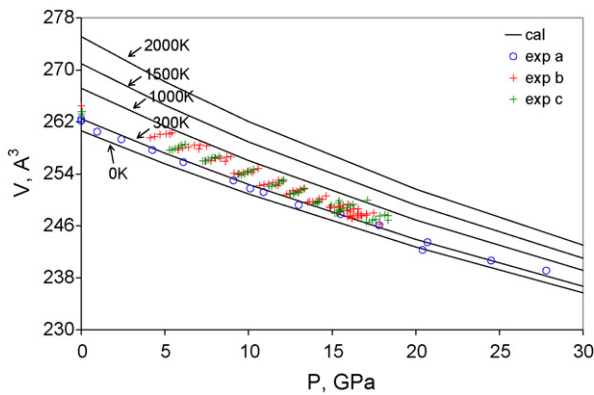
Fig. 2. *P–V–T* relations for akimotoite at high *P–T* from this study and experiments a: (Reynard et al., 1996) at 298 K; b: (Wang et al., 2004) range from 298 K to 773 K; and c: (Wang et al., 2004) range from 298 K to 1373 K.

Fig. 4. Velocity surface of akimotoite at 1500 K.

1996; Wang et al., 2004). It is due to the fact that the compressibility along the *c*-axis is dominated by that of MgO$_6$ octahedra while along the *a*-axis by that of SiO$_6$ octahedra, and MgO$_6$ octahedra are more compressible than SiO$_6$ octahedra (Horiuchi et al., 1982; Wang and Perdew, 1991). Our calculated results provide support for these experimental observations as shown in Fig. 3. As indicated by both calculation and experimental data, firstly, there is a negative dependence on pressure for the *c/a* ratio; secondly, the effect of temperature on the *c/a* ratio is negligible compared with the effect of pressure. The experimental data which are lower than the fitted

line was interpreted as the presence of differential stress (Wang et al., 2004).

The acoustic velocities as a function of crystallographic direction were derived from the calculated single-crystal elastic constants using the Christoffel equation (Nye, 1957), as listed in Table 5. The P wave anisotropy (given as the ratio of maximum velocity to minimum velocity) ranges from 1.09 to 1.20; the S wave anisotropy ranges from 1.13 to 1.55; the shear wave splitting ranges from 1.11 to 1.35. The maximum and minimum P and S wave velocity propagation direction can be seen in Fig. 4. Only 1500 K data at two pressures are plotted since the other *P–T* conditions do not affect the anisotropy dramatically.
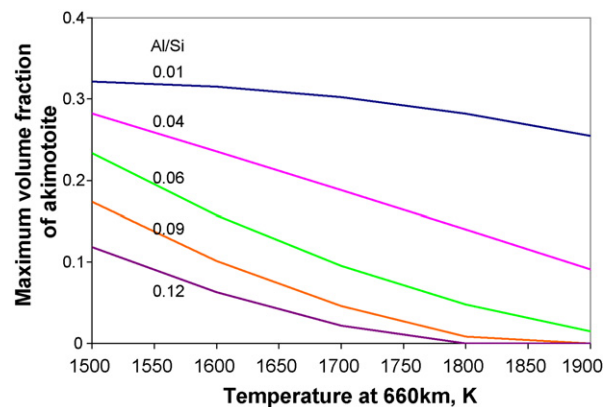

Fig. 3. The *c/a* ratio as a function of pressure for akimotoite; all temperatures are included. Solid diamond symbol data from AIMD calculation range from 0 K to 3000 K, solid line is the fit; experimental data are from a: (Reynard et al., 1996) at 298 K; b: (Wang et al., 2004) range from 298 K to 773 K; and c: (Wang et al., 2004) range from 298 K to 1373 K.
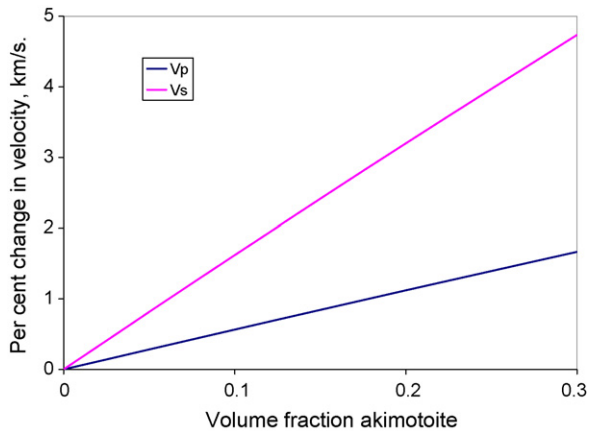

Fig. 5. Volume fraction of akimotoite as a function of temperature and Al/Si ratio. The values are calculated for a pyrolite composition with only aluminium varying from curve to curve using the phase diagram of Gasparik (2003). The geothermal gradient is from Brown and Shankland (1981).

Table 6
Properties of mantle phases at 660 km depth and 1873 K. These values are for the magnesium end-member phase. Values for ringwoodite are from Li et al. (2006a), values for Ca perovskite are from Li et al. (2006b), values for pyrope are from Li et al. (submitted-b), and values for akimotoite are from this study.

|	V_P (km/s)	V_S (km/s)	Density (gm/cm^3)	Shear velocity anisotropy	Volume fraction
Ringwoodite	10.65	5.68	3.79	1.05	0.55
CaSiO$_3$ perovskite	10.54	5.75	4.43	1.50	0.07
Pyrope	10.09	4.91	3.83	1.02	Sums to 0.38
Akimotoite	10.67	5.79	4.04	1.24	

Fig. 6. Effect of akimotoite on seismic velocities at 660 km depth. The volume fraction of akimotoite can be determined from Fig. 5 as a function of composition and temperature.

3.4. Geophysical implications

The stability field of akimotoite depends on both temperature and aluminium content as shown in Fig. 1. Fig. 5 illustrates the maximum volume fraction of akimotoite as a function of the 660 km depth temperature for several Al/Si ratios. A value of 0.12 for this variable is appropriate to pyrolite. Thus, for pyrolite, the temperature must be less than about 1700 K for any akimotoite to be present. Since these phase diagrams are based on iron-free data, some uncertainty is implied, but the overall topology is probably robust.

Table 6 gives estimated properties of the magnesium rich end member of the relevant phases at conditions of the 660 discontinuity. Akimotoite has the largest seismic velocity, being significantly larger than garnet, the phase that it replaces. Fig. 6 illustrates the per cent change in P and S velocity as a function of the akimotoite volume fraction. The shear velocity is much more strongly affected
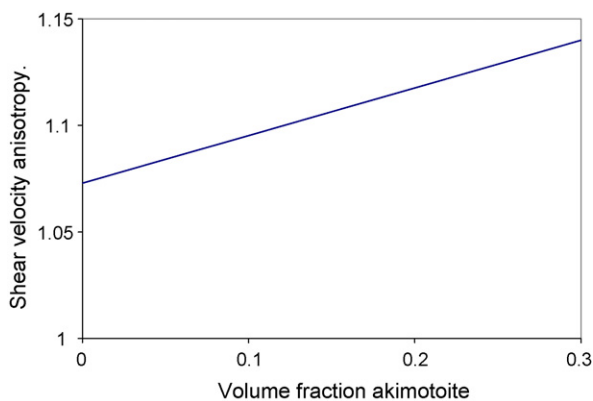
Fig. 7. Effect of akimotoite on maximum shear anisotropy at 660 km depth. The volume fraction of akimotoite can be determined from Fig. 5 as a function of composition and temperature. The anisotropy is the ratio of the maximum to minimum shear velocity for a perfectly aligned mineral assemblage.

than is the P velocity. This may be a useful diagnostic for identifying the presence of akimotoite (Fig. 7).

Table 6 also illustrates the velocity anisotropy expressed as the ratio of the maximum to minimum shear wave velocity. These results using AIMD method agrees with previous classical MD studies (Zhang et al., 2005). At 660 km depth, the Ca perovskite is the most anisotropic phase, but is present in a small amount. Ringwoodite and pyrope are quite isotropic at these conditions. Seismic anisotropy depends not only on the magnitude of this value, but also on the amount of preferred orientation of the mineral grains. The replacement of garnet by akimotoite will increase the maximum possible anisotropy as described by Zhang et al. (2005) and may be a second signature of the presence of akimotoite in the neighbourhood of the 660 km discontinuity.

Acknowledgements

References

Alfè, D., 1999. Ab-initio molecular dynamics, a simple algorithm for charge extrapolation. Computer Physics Communications 118, 31–33.

Allen, M.P., Tildesley, D.J., 1997. Computer Simulation of Liquids. Oxford University Press, New York, NY, 408 pp.

Blöchl, P.E., 1994. Projector augmented-wave method. Physical Review B 50, 17953–17979.

Brown, J.M., Shankland, T.J., 1981. Thermodynamic parameters in the Earth as determined from seismic profiles. Geophysical Journal of the Royal Astronomical Society 66, 579–596.

Da Silva, C.R.S., Karki, B.B., Stixrude, L., Wentzcovitch, R.M., 1999. Ab initio study of the elastic behavior of MgSiO$_3$ ilmenite at high pressure. Geophysical Research Letters 26 (7), 943–946.

Deuss, A., Woodhouse, J., 2001. Seismic observations of splitting of the mid-transition zone discontinuity in Earth's mantle. Science 294 (5541), 354–357.

Gasparik, T., 1990. Phase relation in the transition zone. Journal of Geophysical Research-Solid Earth 95, 15751–15769.

Gasparik, T., 2003. Phase Diagrams for Geoscientists. Springer, 462 pp.

Gossler, J., Kind, R., 1996. Seismic evidence for very deep roots of continents. Earth and Planetary Science Letter 138 (1–4), 1–13.

Gu, Y., Dziewonski, A.M., Agee, C.B., 1998. Global de-correlation of the topography of transition zone discontinuities. Earth and Planetary Science Letter 157 (1–2), 56–67.

Horiuchi, H., Hirano, M., Ito, E., Matsui, Y., 1982. MgsiO$_3$ (ilmenite-type) – single-crystal X-ray-diffraction study. American Mineralogist 67 (7–8), 788–793.

Ito, E., Yamada, H., 1982. Stability relations of silicate spinel ilmenite and perovskites. In: Akimoto, S., Manghnani, M.H. (Eds.), High Pressure Research: Applications to Geophysics. Center for Academic Publishing of Japan, Tokyo, pp. 405–419.

Karki, B.B., Wentzcovitch, R.M., 2002. First-principles lattice dynamics and thermoelasticity of MgSiO$_3$ ilmenite at high pressure. Journal of Geophysical Research-Solid Earth 107 (B11).

Kawai, N., Tachimor, M., Ito, E., 1974. High-pressure hexagonal form of MgSiO$_3$. Proceedings of the Japan Academy 50 (5–6), 378–380.

Kiefer, B., Stixrude, L., Wentzovitch, R.M., 1997. Calculated elastic constants and anisotropy of Mg$_2$SiO$_4$ spinel at high pressure. Geophyscial Research Letters 24 (22), 2841–2844.

Kresse, G., Furthmüller, J., 1996a. Efficiency of ab-initio total energy calculations for metals and semiconductors using a plane-wave basis set. Computation Material Science 6, 15–50.

Kresse, G., Furthmüller, J., 1996b. Efficient iterative schemes for ab initio total-energy calculations using a plane-wave basis set. Physical Review B 54, 11169.

Li, L., Weidner, D.J., Brodholt, J., Alfè, D., Price, G.D., submitted-a. Ab initio molecular dynamic simulation on the elasticity of $Mg_3Al_2Si_3O_{12}$ pyrope. Physics of the Earth and Planetary Interiors.

Li, L., Weidner, D.J., Brodholt, J., Alfè, D., Price, G.D., submitted-b. Ab initio molecular dynamic simulation on the elasticity of $Mg_3Al_2Si_3O_{12}$ pyrope. Physics of the Earth and Planetary Interiors.

Li, L., et al., in press. Elasticity of $CaSiO_3$ perovskite at high pressure and high temperature. Physics of the Earth and Planetary Science.

Li, L., Weidner, D.J., Brodholt, J., Alfè, D., Price, G.D., 2006a. Elasticity of Mg_2SiO_4 ringwoodite at mantle conditions. Physics of the Earth and Planetary Interior 157 (3–4), 181–187.

Li, L., et al., 2006b. Elasticity of $CaSiO_3$ perovskite at high pressure and high temperature. Physics of the Earth and Planetary Science 155 (3–4), 249–259.

Li, L., Weidner, D.J., Brodholt, J., Alfè, D., Price, G.D., 2006c. Elasticity of Mg_2SiO_4 ringwoodite at mantle conditions. Physics of the Earth and Planetary Interiors 157 (3–4), 181–187.

Li, L., Weidner, D.J., Brodholt, J., Price, G.D., 2007. Ab initio study on the effect of cation-ordering and pressure on the elasticity of majorite and majorite-pyrope solid solution. Earth and Planetary Science Letters 256, 28–35.

Matsui, M., Akaogi, M., Matsumoto, T., 1987. Computational model of the structural and elastic properties of the ilmenite and perovskite phases of $MgSiO_3$. Physics and Chemistry of Minerals 14 (2), 101–106.

Nye, J.F., 1957. Physical Properties of Crystals. Oxford University Press, Ely House, London.

Oganov, A.R., Brodholt, J.P., Price, G.D., 2001a. Ab initio elasticity and thermal equation of state of $MgSiO_3$ perovskite. Earth and Planetary Science Letters 184 (3–4), 555–560.

Oganov, A.R., Brodholt, J.P., Price, G.D., 2001b. The elastic constants of $MgSiO_3$ perovskite at pressures and temperatures of the Earth's mantle. Nature (London) 411 (6840), 934–937.

Perdew, J.P., et al., 1992. Atoms, molecules, solids, and surfaces: applications of the generalized gradient approximation for exchange and correlation. Physical Review B 46, 6671–6687.

Reynard, B., Fiquet, G., Itie, J.P., Rubie, D.C., 1996. High-pressure X-ray diffraction study and equation of state of MgSiO3 ilmenite. American Mineralogist 81 (1–2), 45–50.

Reynard, B., Rubie, D.C., 1996. High-pressure, high-temperature Raman spectroscopic study of ilmenite-type MgSiO3. American Mineralogist 81 (9–10), 1092–1096.

Tachimori, M., Kawai, N., Ito, E., 1975. High-pressure hexagonal form of $MgSiO_3$. Review of Physical Chemistry of Japan, 215–1215.

Wang, Y., Perdew, J.P., 1991. Correlation hole of the spin-polarized electron-gas, with exact small-wave-vector and high density scaling. Physical Review B 44, 13298–13307.

Wang, Y., Uchida, T., Zhang, J., Rivers, M.L., Sutton, S.R., 2004. Thermal equation of state of akimotoite MgSiO3 and effects of the akimotoite–garnet transformation on seismic structure near the 660 km discontinuity. Physics of the Earth and Planetary Interiors 143–144, 57–80.

Weidner, D.J., Ito, E., 1985. Elasticity of $MgSiO_3$ in the ilmenite phase. Physics of the Earth and Planetary Interiors 40 (1), 65–70.

Weidner, D.J., Wang, Y., 2000. Phase transformations: implications for mantle structure. AGU Monography, Mineral Physics and Tomography from the Atomic to the Global Scale Geophysical Monograph 117, 215–235.

Zhang, Y.G., Zhao, D.P., Matsui, M., 2005. Anisotropy of akimotoite: a molecular dynamics study. Physics of the Earth and Planetary Interiors 151 (3–4), 309–319.